

Zinc isotope fractionation under vaporization processes and in aqueous solutions

Jixi Zhang^{1,2} · Yun Liu²

Received: 25 January 2018 / Revised: 10 June 2018 / Accepted: 27 June 2018 / Published online: 17 July 2018
© Science Press, Institute of Geochemistry, CAS and Springer-Verlag GmbH Germany, part of Springer Nature 2018

Abstract Equilibrium Zn isotope fractionation was investigated using first-principles quantum chemistry methods at the B3LYP/6-311G* level. The volume variable cluster model method was used to calculate isotope fractionation factors of sphalerite, smithsonite, calcite, anorthite, forsterite, and enstatite. The water-droplet method was used to calculate Zn isotope fractionation factors of Zn^{2+} -bearing aqueous species; their reduced partition function ratio factors decreased in the order $[\text{Zn}(\text{H}_2\text{O})_6]^{2+} > [\text{ZnCl}(\text{H}_2\text{O})_5]^+ > [\text{ZnCl}_2(\text{H}_2\text{O})_4] > [\text{ZnCl}_3(\text{H}_2\text{O})_2]^- > \text{ZnCl}_4^{2-}$. Gaseous ZnCl_2 was also calculated for vaporization processes. Kinetic isotope fractionation of diffusional processes in a vacuum was directly calculated using formulas provided by Richter and co-workers. Our calculations show that in addition to the kinetic isotope effect of diffusional processes, equilibrium isotope fractionation also contributed nontrivially to observed Zn isotope fractionation of vaporization processes. The calculated net Zn isotope fractionation of vaporization processes was 7–7.5‰, with ZnCl_2 as the gaseous species. This matches experimental observations of the range of Zn isotope distribution of lunar samples. Therefore, vaporization processes may be the cause of the large distribution of Zn isotope signals found on the Moon. However, we cannot further distinguish the origin of such vaporization processes; it might be due either to igneous rock melting in

meteorite bombardments or to a giant impact event. Furthermore, isotope fractionation between Zn-bearing aqueous species and minerals that we have provided helps explain Zn isotope data in the fields of ore deposits and petrology.

Keywords Evaporation process · Zinc isotope · Kinetic isotope fractionation · Equilibrium fractionation · Zinc species in solution

1 Introduction

Zinc (Zn) is a transition element with atomic number 30. Its abundance in the upper continental crust is about 71 µg/g (Taylor and McLennan 1995; Cloquet et al. 2008). Zinc is the second most abundant transition metal in the deep ocean, with a concentration of up to 15 nmol/L (Cloquet et al. 2008). In nature, Zn mainly exists in sulfides; the predominant Zn-bearing mineral is sphalerite (cubic ZnS), with smithsonite (ZnCO_3) and hemimorphite also fairly common.

Zinc has five stable isotopes— ^{64}Zn , ^{66}Zn , ^{67}Zn , ^{68}Zn , and ^{70}Zn —with abundances of 49.19%, 27.79%, 4.04%, 18.39%, and 0.60%, respectively (Tanimizu et al. 2002). The average atomic mass of Zn is 65.37777 (Ponzevera et al. 2006), but there is controversy over its absolute value (Rosman 1972, b); Chang et al. (2001). Blix et al. (1957) and Rosman (1972) were the pioneers in studying Zn content of different samples. At the time, they found no Zn isotope composition changes in terrestrial samples due to limitations of available analysis techniques. However, with the development of multiple collector-inductively coupled plasma-mass spectrometry (MC-ICP-MS), isotope analysis precision has increased substantially, enabling us to make more precise measurements of Zn isotope composition.

✉ Yun Liu
liuyun@vip.gyig.ac.cn

¹ School of Karst Science, Guizhou Normal University/State Engineering Technology Institute for Karst Desertification Control, Guiyang 550001, China

² State Key Laboratory of Ore Deposit Geochemistry, Institute of Geochemistry, Chinese Academy of Sciences, Guiyang 550081, China

Maréchal et al. (1999) first utilized ICP-MS to analyze Zn isotope composition of terrestrial and biological samples. Their results indicate that Zn isotope composition variations are common in natural samples. In the past several years, the study of Zn isotopes has been widely applied to many fields, such as astrochemistry (Luck et al. 2005, 2006; Moynier et al. 2006, 2007; Herzog et al. 2009, 2010, 2011), geology (Maréchal et al. 1999; Mason et al. 2005; Wilkinson et al. 2005; John et al. 2008; Moynier et al. 2009; Pons et al. 2013), environmental chemistry (Bermin et al. 2006; Vance et al. 2006; Weiss et al. 2007), and biology (Maréchal and Albarède 2002; Zhu et al. 2002).

It is noteworthy that Zn is a moderately volatile element, i.e., with a half-mass condensation temperature (T_c) (at 10^{-4} bar) between 1250 and 650 K (Palme et al. 1988). The moderate volatile elements include P, Mn, Li, As, Sb, Ga, Na, Cl, B, Ge, Rb, F, Zn, Te, Sn, Se, and S. Several different T_c results of Zn have been published: 684 K at 10^{-4} bar, 668 K at 10^{-6} bar (Wai and Wasson 1977), and about 730 K at 10^{-4} bar (Lodders 2003). These results suggest that Zn-bearing species can be volatilized and sublimated to the gas phase easily at temperatures of 400–700 °C.

The study of Zn isotope fractionation opens a door to investigate the details of evaporation processes in which Zn-bearing compounds are involved. Volatile elements play a key role in the chemical evolution of planets. From previous studies we know that the Moon is volatile-depleted and stable isotope fractionation of moderately volatile elements could have happened during the giant impact event of Moon formation (Humayun and Clayton 1995; Albarède 2009). Previous studies have also shown that Zn isotopes could be largely fractionated in vaporization processes of other terrestrial planetary bodies (e.g. Moon), but only marginally fractionated during igneous processes of the Earth (Moynier et al. 2006, 2009, 2011; Albarède 2009; Paniello et al. 2012). Therefore, Zn has become a very popular element in investigations of the evaporation processes associated with the giant impact. In addition, Zn isotope fractionation has been found to be larger in samples with low Zn concentrations than those with high Zn concentrations; in other words, the isotope composition of Zn is negatively correlated to elemental abundance (Paniello et al. 2012).

Isotope tracing is an important method in ore deposit investigation. From the perspective of metallogeny, traditional stable isotopes such as H, C, O, and S are often indirectly related to the source of metals, i.e., the main body of ore deposits. Therefore, more and more studies are using non-traditional isotope systems (e.g., Cu, Fe, Zn) to study ore deposits. In the past several years, developments

in Zn isotope analysis techniques have made it possible to utilize Zn isotopes to trace the formation of Zn-bearing deposits (Albarède 2004; Mason et al. 2005; Wilkinson et al. 2005; John et al. 2008). However, these studies indicate that Zn isotope fractionation is small (< 0.5‰) relative to other transition metals (those having more than two redox states) such as Fe (about 5‰). This is because Zn has only one common oxidation state (Zn^{2+}) (Dauphas and Rouxel 2006; Gagnevin et al. 2012).

Meanwhile, Zn plays an important role in the interaction between biosphere and geosphere. If the concentration of Zn exceeds a threshold, it can cause environmental pollution. The study of Zn distribution has a number of applications in investigations of organic evolution and environmental pollution (Novak et al. 2016).

In this study, we used quantum chemistry to obtain basic Zn isotope fractionation factors of different Zn-bearing substances. These factors can be useful for people studying Zn isotopes in several geoscience subdisciplines. We also applied these Zn isotope fractionation factors to explain the vaporization processes observed on the Moon.

2 Theory and methods

2.1 Equilibrium isotope fractionation calculation

The Bigeleisen–Mayer equation or Urey model (Bigeleisen and Mayer 1947; Urey 1947) is the cornerstone of theoretical and computational stable isotope geochemistry, revealing the equilibrium isotope exchange constant K . Take a simple isotope exchange reaction as an example:



where A and B stand for two kinds of substances, A^* and B^* are the substance with heavier isotopes relative to A and B , respectively. The reaction equilibrium constant, K , can be obtained from the ratio of the reduced partition function ratios (RPFRs) of these two substances:

$$K = \frac{RPFR(A)}{RPFR(B)} \quad (2)$$

In the field of geochemistry, the isotope fractionation factor, α , is used instead of K . The relationship between α and K is $\alpha = K^{1/n}$, where n is the number of atoms exchanged during the isotopic exchange reaction. If there is only one isotope exchanged during the reaction, then $\alpha = K$. In most cases, because α is very close to 1.0, the isotope fractionation factor between A and B is approximately $\Delta_{A-B} \approx 10^3 * \ln\alpha$. The expression of RPFR can be calculated as:

$$\left(\frac{s}{s^*}\right)RPFR = \prod_i^{3n-6} \frac{u_i \exp(-u_i/2)}{u_i^* \exp(-u_i^*/2)} \frac{1 - \exp(-u_i^*)}{1 - \exp(-u_i)} \quad (3)$$

where s is the symmetry number of the molecules or clusters. In this study, $s = s^*$. The asterisk stands for the molecules with heavier isotopes. And u_i can be obtained from the harmonic vibrational frequencies, v_i :

$$u_i = \frac{hv_i}{k_b T} \quad (4)$$

where h , k_b , and T are the Planck constant, the Boltzmann constant, and temperature in Kelvin, respectively. Based on this model, the equilibrium isotope fractionation factor can be obtained via the harmonic vibrational frequencies of two substances and the magnitude of isotope fractionation is related to the temperature. Under extremely high temperature, isotope fractionation will be very small and even become negligible.

One of the key factors in isotope fractionation calculation is precise harmonic frequencies of different isotopologues. With the tremendous developments in computational quantum chemistry, it is possible to calculate the harmonic vibrational frequencies of macromolecules, molecule clusters, and even condensed phases. Those harmonic frequencies are exactly what the Bigeleisen–Mayer equation requires (Liu et al. 2010). Consequently, using ab initio or first-principles methods to calculate isotope fractionation factors is becoming a routine job (Driesner and Seward 2000; Oi 2000; Oi and Yanase 2001; Jarzecki et al. 2004; Schauble 2004; Anbar et al. 2005; Liu and Tossell 2005; Tossell 2005; Zeebe 2005; Schauble et al. 2006; Rustad and Bylaska 2007; Schauble 2007; Seo et al. 2007; Otake et al. 2008; Rustad et al. 2008; Rustad and Zarzycki 2008; Fujii et al. 2009a, b, 2010, 2011; Fujii and Albarède 2012; Li et al. 2009; Li and Liu 2011; Li and Liu 2010; Black et al. 2011; Pons et al. 2013). Researchers often need to implement scaling treatment to obtain reasonable harmonic vibrational frequencies of different molecules (Hehre 1986). Several previous studies focused on improving the Bigeleisen–Mayer equation by adopting higher-level anharmonic corrections (Richet et al. 1977; Bigeleisen 1996, 1998; Liu et al. 2010). For a transition metal isotope system like Zn, its anharmonicity is small and those corrections are unnecessary. In this study, Gaussian03 and Gaussian09 software were used for all calculations (Frisch et al. 2003, 2009).

2.2 Isotope fractionation calculation of diffusion process in vacuum

Both equilibrium and physical kinetic processes can affect isotope fractionation. Here, we introduce methods to calculate diffusional isotope fractionation, which is a physical kinetic process. The theoretical expression of the molecular diffusion coefficient is defined from the Chapman–Enskog theory (Chapman and Cowling 1991):

$$D_m = \frac{3}{8N\sigma_0} \sqrt{\frac{kT(m+M)}{2\pi m M}} \quad (5)$$

where D_m , N , M , and T are the molecular diffusion coefficient, atmospheric density, average mass of the environmental material, and temperature in Kelvin, respectively. σ_0 is a factor depending on the collision integral and molecular radius, and m is the mass of the interested atom.

In the gas phase, the widely used definition of the isotope fractionation factor during the diffusion process is equal to the quotient of the molecular diffusion coefficients of different isotopologues:

$$\alpha^{kin} = \frac{D_{m_H}}{D_{m_L}} = \sqrt{\frac{m_L(m_H + M)}{m_H(m_L + M)}} \quad (6)$$

where m_H and m_L are the particles (molecules) with heavy and light isotope atoms, respectively. If the molecules are diffused into a vacuum, M is approximately equal to the lighter isotopologues. In other words, $M \approx m_L$. Therefore,

$$\alpha^{kin} = \sqrt{\frac{m_L}{m_H}} \sqrt{\frac{m_H + m_L}{2m_L}} \quad (7)$$

The expression above is similar to the equation obtained by Richter et al. (2007):

$$\alpha_{ik}^{kin} = \sqrt{\frac{m_k}{m_i}} \quad (8)$$

where i and k indicate particles with atoms of different atomic mass. In fact, the term of the kinetic isotope fractionation factor includes the evaporation coefficient ratio of different isotopologues (i.e. γ_i/γ_k) where γ is the evaporation coefficient. There is an assumption that different isotopologues of a given element have similar evaporation coefficients (Richter et al. 2007). Equation (8) has been used by a lot of researchers in the domain of geochemistry and astrochemistry (Davis et al. 1990; Richter et al. 2002, 2007, 2009; Young and Galy 2004; Paniello et al. 2012).

Richter et al. (2007) deduced the expression of isotope fractionation factor of evaporation processes through the method of flux, and indicated that it could be divided into two parts—equilibrium fractionation and physical kinetic fractionation, i.e.:

$$\alpha^{evap} = \alpha^{eq} * \alpha^{kin} \quad (9)$$

where α^{evap} , α^{eq} , and α^{kin} are the total isotope fractionation factor during the evaporation process, the equilibrium fractionation factor, and the kinetic fractionation factor, respectively. The equilibrium fractionation factor can be calculated through the Urey model, which will be illustrated in the following section.

2.3 The volume variable cluster model method

In this study, Zn-bearing minerals were simulated by a cluster-model-based method, known as the volume variable cluster model (VVCM) method (He and Liu 2015; Li and Liu 2015; He et al. 2016). Molecular clusters can be used to represent mineral environments (Gibbs 1982). The isotope effect is indeed a local effect mostly affected by the next nearest neighborhood atoms (i.e., the NNN rule). With a cluster size larger than this threshold, the isotope effect of the interested atom can be properly addressed.

VVCM was proposed to improve a similar method suggested by Rustad et al. (2010). The largest difference between them is that a fixed layer of atoms in the model of Rustad et al. (2010) has been removed and all the atoms in the VVCM are freely optimized. This treatment is used to remedy possible false tensions produced by fixed-volume treatment and the use of different theoretical levels for aqueous and solid species. Under VVCM, the whole cluster is freely optimized to the lowest energy point and the same theoretical level is used for both aqueous and solid species.

For VVCM, several rules must be followed to produce reasonable results. First, the interested atom (here, Zn) is always placed at the center of the cluster model. Second, hundreds of virtual charges are needed around the cluster to electronically neutralize it. The distance and positions of the outmost atoms and virtual charges are adjustable to let the cluster find a minimal energy point from full optimization. The B3LYP/6-311G* level was used for all Zn-bearing species studied here. Cluster models of sphalerite, anorthite, enstatite, and calcite with Zn atoms at the center are shown in Fig. 1.

2.4 The solvation effect calculation

In this study, the water-droplet method was used to model the solvation effect in aqueous solutions, i.e., Zn^{2+} cation was surrounded by a number of water molecules or ligands to model its chemical environment in solution. For example, when attempting to calculate Zn^{2+} in diluted aqueous solutions, its first coordination shell structure must be based on experimental evidence. Because $[Zn(H_2O)_6]^{2+}$ is the dominant species of aqueous Zn^{2+} (Black et al. 2011), we first put six water molecules surrounding the Zn^{2+} ion

to form an octahedral-like structure. These six water molecules were treated as the first shell of waters of this complex. After optimizing this structure, another six water molecules were added to the optimized $[Zn(H_2O)_6]^{2+}$ structure to form $[Zn(H_2O)_6]^{2+}(H_2O)_6$. These new water molecules were all placed at the second-coordination shell of Zn^{2+} . Then this structure was optimized again. By this procedure, we obtained the most stable structure of $[Zn(H_2O)_6]^{2+}(H_2O)_{24}$, and then calculated its harmonic vibrational frequencies. Note that the geometry optimization and frequency calculation processes must be under the same theoretical level. Even though significant time was required to optimize geometries and calculate frequencies, from our experience, it is improper to pre-optimize the geometry at a lower level first, then re-optimize it at a higher level in order to save time. Inaccurate local structures are often produced by lower theoretical levels and cannot be corrected under higher levels due to the minimal search limitation of current methods.

3 Results and discussion

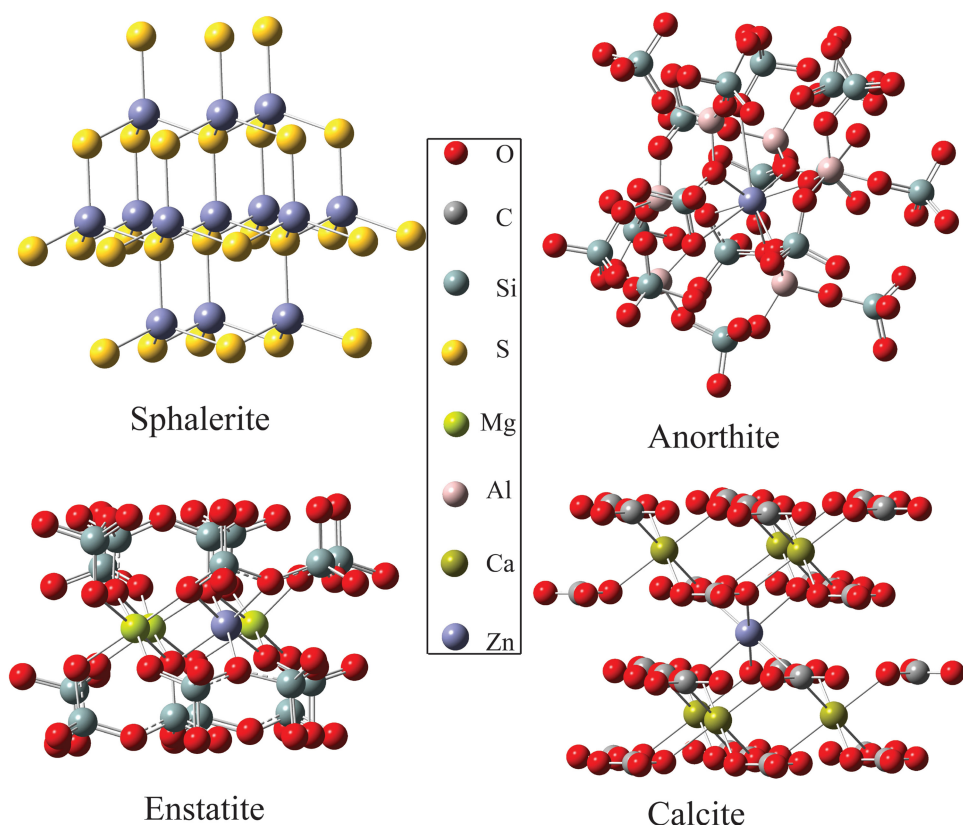
3.1 Zinc isotope fractionation in the evaporation process

3.1.1 Equilibrium zinc isotope fractionation in the evaporation process

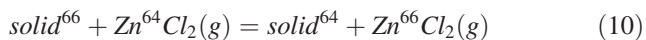
The Earth and Moon have identical isotope compositions of oxygen and refractory elements such as Cr, W, and Ti. The results of Paniello et al. (2012) indicate that the isotopic compositions of volatile elements on the Moon are very different from those of Earth. The variation range of lunar sample isotope compositions is up to 8%, while it is mostly around zero for Martian meteorites and terrestrial igneous rocks. They attributed these differences to the evaporation caused by the Moon-forming giant impact event, during which the Moon was enriched with heavy Zn isotopes. On the planetary scale, Zn is one of the few elements that is different in lunar and terrestrial basalt samples. This difference may be caused by evaporation processes, as many studies have suggested that magmatic differentiation could not cause large Zn isotope fractionation.

Evaporation (similar to condensation) is a very important process for studying the formation of the Moon and the chemical evolution of planets. There have been many studies on isotopic fractionation during evaporation or condensation (Luck et al. 2005, 2006; Moynier et al. 2006, 2007, 2010, 2011; Herzog et al. 2009; Paniello et al. 2012). Data from meteorites indicate that Zn is compatible with Mg in silicates and anorthite, which are the main hosts

Fig. 1 Cluster models of sphalerite, anorthite, enstatite, and calcite with Zn atoms at the center



of Zn in lunar samples. Therefore, we chose to analyze forsterite, enstatite, and anorthite by VVCM with the center metal atoms substituted by Zn (Lodders 2003; Liu et al. 2006) to simulate these Zn-bearing solid minerals. The RPFRs of these minerals decreased in the sequence enstatite > forsterite > anorthite (Fig. 2). Previous results have shown that the evaporation product of Zn was $ZnCl_2(g)$ (Chou et al. 1975). Hence, we considered the whole isotopic exchange reaction during the evaporation as:



The equilibrium isotope fractionation factors between the solid phases and gas phase were obtained through the Bigeleisen–Mayer equation. The relationship between the equilibrium fractionation factors and temperatures is shown in Fig. 3. These results show that during the evaporation processes, the gaseous phase ($ZnCl_2$) preferentially enriched heavier Zn isotopes relative to the solid phase except for enstatite, which slightly enriched heavier isotope relative to $ZnCl_2$. The magnitudes of equilibrium Zn isotope fractionation between gas and condensed phases were about +0.3, +2 and -0.18‰ at 25 °C for forsterite, anorthite, and enstatite, respectively. Isotope fractionation decreases as temperature increases and if the temperature is

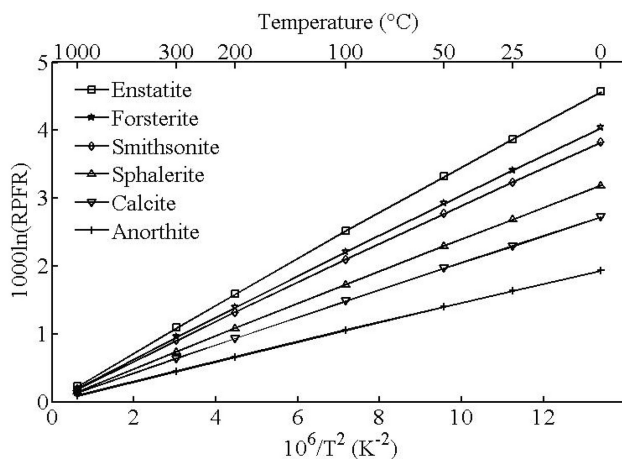


Fig. 2 Reduced partition function ratios of enstatite, forsterite, smithsonite, sphalerite, calcite, and anorthite (the center atoms are substituted by Zn) as a function of temperature at B3LYP/6-311G* level

high enough, the equilibrium isotopic fractionation becomes negligible.

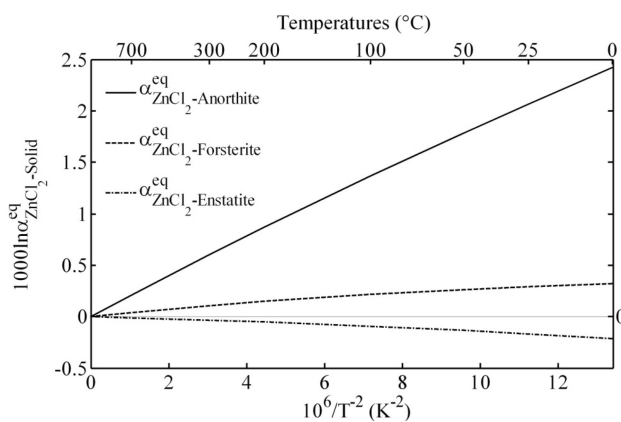


Fig. 3 Equilibrium Zn isotope fractionation factors versus temperature at the B3LYP/6-311G* level

3.1.2 The total isotope fractionation of zinc during evaporation processes

For a process like Zn-bearing compounds evaporating in a vacuum, the kinetic isotope fractionation factor can be calculated using Eq. (8). In this study, the gas species was $\text{ZnCl}_2(\text{g})$. The kinetic Zn isotope fractionation factor caused by diffusion in a vacuum was about 0.993. The total isotope fractionation factor of Zn during the evaporation process is approximately equivalent to the equilibrium isotope fractionation factor times the kinetic fractionation factor, i.e., $\alpha^{\text{evap}} = \alpha^{\text{eq}} * \alpha^{\text{kin}}$ (Richter et al. 2007). The fractionation factors of Zn-bearing substances during evaporation processes are plotted as a function of temperature in Fig. 4.

If there is a reservoir effect, Zn isotope fractionation between vapor and condensed phases can be determined using the Rayleigh distillation model:

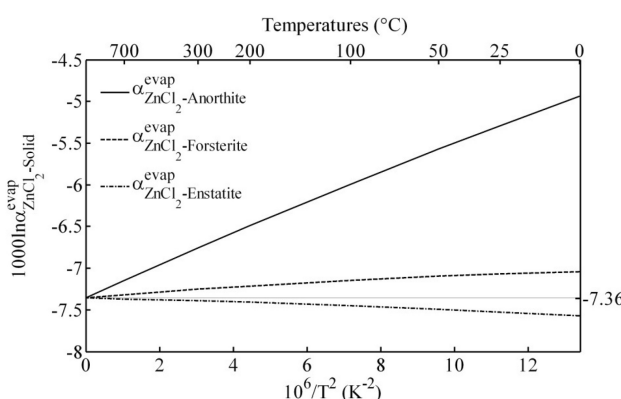


Fig. 4 Zn isotope fractionation factors of evaporation processes between gaseous ZnCl_2 and solid phases as a function of temperature

$$R_{(\text{residual})} = R_0 f^{\alpha^{\text{evap}} - 1} \quad (11)$$

where R is the isotopic ratio of the residual (solid) phase, R_0 the initial isotopic ratio of the isotope, f the fraction of this isotope remaining in the condensed phase, and α^{evap} the apparent isotope fractionation factor of the whole evaporation process. If Rayleigh fractionation is expressed in the form of δ , then

$$\delta_{\text{final}} = \delta_{\text{initial}} + \left[(1000 + \delta_{\text{initial}}) (f^{(\alpha-1)} - 1) \right] \quad (12)$$

where the subscripts “final” and “initial” stand for the isotope compositions of the final and initial state in units of permil (‰). In most experimental situations, the initial isotope composition, δ , of Zn is known and the isotope composition of the final state can be acquired by experimental method, hence the fraction of isotope remaining in the condensed phase can be calculated.

In previous study, the isotope fractionation factor of Rayleigh distillation only used the square-root of the mass of different isotopologues. However, the experimental values are smaller than the theoretical ones. In our method, we introduced the equilibrium isotope fractionation factor into the isotope fractionation factor of evaporation used in the Rayleigh equation. We offer a theoretical explanation that equilibrium isotopic fractionation could vary in a negative direction to kinetic isotopic fractionation. Previous studies have suggested that the isotope fractionation factor of the evaporation process is 0.993; however, our results indicate that equilibrium isotope fractionation (of forsterite and especially anorthite) also plays a nontrivial role in the overall fractionation of the evaporation process (Fig. 4), largely because Zn can be vaporized at lower temperatures. In the case of enstatite, the total isotope fractionation factor was slightly higher than the kinetic isotope fractionation factor. Previous research has shown that the vast majority of plagioclase is anorthite in Moon rock samples; hence, the total isotope fractionation factor would be smaller if we considered equilibrium isotope fractionation.

The calculated net Zn isotope fractionation of vaporization processes was about 7–7.5‰ (Fig. 4), with ZnCl_2 as the gaseous species. This matches the experimental observations of the range of Zn isotope distribution of lunar samples (e.g., Paniello et al. 2012). Therefore, vaporization processes may be the cause of the large distribution of Zn isotope signals found on the Moon. However, we cannot further distinguish the origin of such vaporization processes. It might be due either to common igneous rock melting or to a giant impact event.

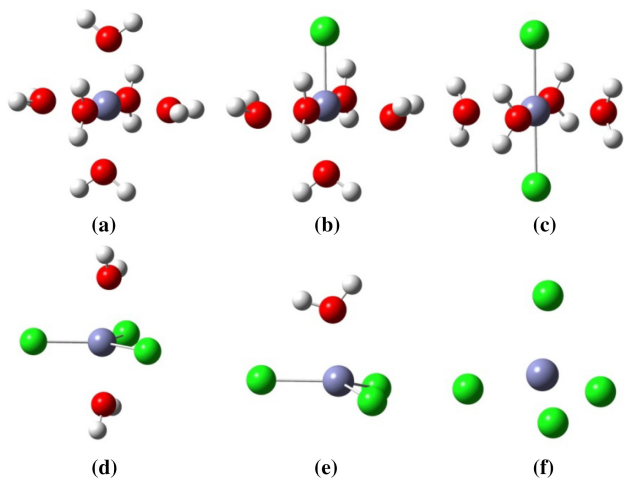


Fig. 5 The first coordination shells of Zn^{2+} in aqueous solution. **a–f** represent the aqueous species of $[\text{Zn}(\text{H}_2\text{O})_6]^{2+} \cdot 24\text{H}_2\text{O}$, $[\text{ZnCl}(\text{H}_2\text{O})_5]^+ \cdot 24\text{H}_2\text{O}$, $[\text{ZnCl}_2(\text{H}_2\text{O})_4] \cdot 24\text{H}_2\text{O}$, $[\text{ZnCl}_3(\text{H}_2\text{O})]^- \cdot 24\text{H}_2\text{O}$, $[\text{ZnCl}_3(\text{H}_2\text{O})]^- \cdot 24\text{H}_2\text{O}$, and $[\text{ZnCl}_4]^{2-} \cdot 24\text{H}_2\text{O}$, respectively. Zinc atoms are shown in indigo; oxygen in red; chlorine in green; and hydrogen in white

3.2 Speciation and isotope fractionation factors of Zn^{2+} in aqueous solutions

One of the reasons that Zn isotope compositions have a small distribution for Earth samples is that there is water on Earth. Zinc can be easily dissolved into solution, especially brines. From experiments, direct structure information about aqueous Zn species can be obtained through visible, infrared, and ultraviolet spectra; Raman spectrum; X-ray diffraction; X-ray absorption; and neutron scattering. Most of these studies require a relatively large number of samples for analysis. Anderson et al. (1998) pioneeringly used X-ray absorption fine structure (XAFS) to investigate metal halide in fluid inclusions.

The speciation of Zn^{2+} in aqueous solutions is related to the different types of ligands, ligand concentrations, and pH (Maréchal and Albarède 2002; Black et al. 2011). Liu et al. (2011) used ab initio molecular dynamics to investigate the hydration of Zn^{2+} in hydrothermal fluids. Investigations of natural fluid inclusions have indicated that the predominant species in hyper-saline brines up to 430 °C is tetrahedral ZnCl_4 (Anderson et al. 1995, 1998), a finding confirmed qualitatively by Mayanovic et al. (1999). However, in most cases, the chief speciation of Zn^{2+} complex is $[\text{Zn}(\text{H}_2\text{O})_6]^{2+}$ in diluted aqueous solutions (Black et al. 2011). In addition, the coordination between Zn^{2+} and other inorganic ligands (such as chloridion, hydrogen sulfide, and hydroxyl) are also very important because water molecules are always replaced by halogen or sulfide species or other anionic ligands in ore-forming

fluids or seawater (Liu et al. 2011). Therefore, the coordination forms of Zn complexes in brine are very complicated; meanwhile, the concrete geometries of Zn complexes play a key role in understanding the geochemical behavior of Zn^{2+} cations.

The optimized first-coordination shell structures of different aqueous Zn^{2+} species are shown in Fig. 5, and their Zn–O and Zn–Cl bond-length results are shown in Table 1. From the optimized geometries and previous studies on aqueous Zn^{2+} complexes (Black et al. 2011), a conclusion could be drawn that aqueous Zn^{2+} is always hexa-coordinated with water molecules (i.e., $[\text{Zn}(\text{H}_2\text{O})_6]^{2+}$). Otherwise, if there are Cl^- ions in the first coordination shell of Zn^{2+} , it can be 6-, 5-, or 4-coordinated, such as $[\text{ZnCl}_2(\text{H}_2\text{O})_4]$, $[\text{ZnCl}_3(\text{H}_2\text{O})_2]^-$, and $[\text{ZnCl}_4]^{2-}$.

The optimized geometry of $[\text{Zn}(\text{H}_2\text{O})_6]^{2+}$ places it in the symmetry point group T_h (Fig. 5). The optimized Zn–O bond length was about 2.10 Å, slightly larger than experimental results (2.08–2.09 Å), but better than results obtained by a previous calculation (Parchment et al. 1996). Table 1 shows optimized Zn–O and Zn–Cl bond lengths of all aqueous Zn species studied. In the structure of $[\text{ZnCl}(\text{H}_2\text{O})_5]^+$, the five Zn–O bonds were slightly different from each other and the axial Zn–O (2.06 Å) bond was very close to the experimental value (2.07 Å).

Owing to the importance of understanding Zn isotope fractionation in natural samples, it is necessary to study Zn isotope fractionation in solution systematically. Researchers have found that the different forms of metal-bearing species can affect isotopic fractionation (Hill et al. 2009; Fujii et al. 2010). The complexes of Zn^{2+} in aqueous solutions coordinated with chloridion were calculated by Fujii et al. (2009a, b, 2010). Schauble (2003) researched Zn isotope fractionation factors between minerals and Zn^{2+} aqueous solutions and the latest article about the theoretical calculation of Zn isotopes is by Black et al. (2011).

Complexes with different ligands or different coordination numbers of the same ligands have different isotope fractionation factors. A different number of ligands (such as water) in the inner layer of complexes in aqueous solutions can also produce various isotope fractionation factors. Therefore, the isotope fractionation factors between different Zn-bearing species which exist in aqueous solutions and their precipitated solids (e.g., ZnS , ZnCO_3 , and Zn(O)) will be absolutely different.

In this study, we mainly investigated the complexes of Zn that coordinated with water and chlorine. In most Zn^{2+} –Cl aqueous solutions, the possible species are $[\text{Zn}(\text{H}_2\text{O})_6]^{2+}$, $[\text{ZnCl}(\text{H}_2\text{O})_5]^+$, $[\text{ZnCl}_2(\text{H}_2\text{O})_4]$, $[\text{ZnCl}_3(\text{H}_2\text{O})_2]^-$, and $[\text{ZnCl}_4]^{2-}$. To obtain more accurate and reasonable results, four different possible local configurations were used to simulate Zn^{2+} aqueous species (with subscripts A, B, C, and D). These species were surrounded by up to 24

Table 1 Calculated and experimental bond lengths of different Zn^{2+} species in aqueous solutions

Species	Bond	Bond length (\AA)		Exp. results	
		Theoretical results			
		Parchment et al. (1996)	This study		
$[Zn(\text{H}_2\text{O})_6]^{2+}$	Zn–O	2.14	2.10	2.08–2.09 ^a	
$[Zn\text{Cl}(\text{H}_2\text{O})_5]^+$	Zn–O	2.16, 2.19, 2.20, 2.21	2.15, 2.16, 2.17, 2.06	2.07 ^b	
	Zn–Cl	2.27	2.26	2.24 ^b	
$[Zn\text{Cl}_2(\text{H}_2\text{O})_4]$	Zn–O	2.22	2.16		
	Zn–Cl	2.35	2.35		
$[Zn\text{Cl}_3(\text{H}_2\text{O})_2]^-$	Zn–O	2.37	2.16		
	Zn–Cl	2.32, 2.39	2.32, 2.50		
$[Zn\text{Cl}_3(\text{H}_2\text{O})]^-$	Zn–O	2.28	2.16		
	Zn–Cl	2.26, 2.32	2.27, 2.32		
$[Zn\text{Cl}_4]^{2-}$	Zn–Cl	2.39	2.39	2.28 ^c	

^aBol et al. (1970) and Magini et al. (1988)^bPaschina et al. (1983)^cKruh and Standley (1962)

water molecules to include solvation effects. Before arriving at the final structure of Zn^{2+} complexes such as $[Zn(\text{H}_2\text{O})_6]^{2+} \cdot 24\text{H}_2\text{O}$, a series of water-droplets were optimized with 6, 12, and 18 water molecules. The RPFRs of the four different configurations were slightly different from each other although they were surrounded by the same number of water molecules (see Table 2). All the structures of these water-droplet clusters are shown in Fig. 6. The average RPFR value of the four different configurations was taken as the final result (see Fig. 7).

The results show that the RPFRs of different Zn^{2+} species decreased with an increased number of chlorine ligands, i.e., $[Zn(\text{H}_2\text{O})_6]^{2+} \cdot 24\text{H}_2\text{O}$ had the biggest RPFR, while $[Zn\text{Cl}_4]^{2-} \cdot 24\text{H}_2\text{O}$ had the smallest. This can be explained by the difference between the different ligands, i.e., H_2O and Cl. Our calculation level was different from that used in Black et al. (2011). Our results were slightly different from those of Black et al. (2011). Taking the RPFR of $[Zn(\text{H}_2\text{O})_6]^{2+} \cdot 24\text{H}_2\text{O}$ (0 °C) as an example, their results are 4.42, 4.41, 4.55, 4.50, and 4.49 (B3LYP/LANL2DZ & 6-31G*) while our results were 4.70, 4.56,

Table 2 Calculated $1000 * \ln(\text{RPFR})$ values (in terms of $^{66}\text{Zn}/^{64}\text{Zn}$) for $[Zn(\text{H}_2\text{O})_6]^{2+} \cdot 24\text{H}_2\text{O}$, $[Zn\text{Cl}(\text{H}_2\text{O})_5]^+ \cdot 24\text{H}_2\text{O}$, $[Zn\text{Cl}_2(\text{H}_2\text{O})_4] \cdot 24\text{H}_2\text{O}$, $[Zn\text{Cl}_3(\text{H}_2\text{O})_2]^- \cdot 24\text{H}_2\text{O}$, and $[Zn\text{Cl}_4]^{2-} \cdot 24\text{H}_2\text{O}$

T (°C)	$[Zn(\text{H}_2\text{O})_6]^{2+} \cdot 24\text{H}_2\text{O}$				$[Zn\text{Cl}(\text{H}_2\text{O})_5]^+ \cdot 24\text{H}_2\text{O}$				$[Zn\text{Cl}_2(\text{H}_2\text{O})_4] \cdot 24\text{H}_2\text{O}$			
	A	B	C	D	A	B	C	D	A	B	C	D
0	4.70	4.56	4.74	4.74	4.31	4.33	4.36	4.40	4.16	4.41	4.34	4.30
25	3.99	3.87	4.02	4.02	3.65	3.67	3.69	3.73	3.53	3.73	3.68	3.64
50	3.42	3.32	3.45	3.45	3.13	3.15	3.17	3.21	3.03	3.21	3.16	3.13
100	2.60	2.52	2.62	2.62	2.38	2.39	2.41	2.44	2.31	2.43	2.40	2.37
200	1.64	1.59	1.66	1.66	1.50	1.51	1.52	1.54	1.46	1.54	1.52	1.50
300	1.13	1.09	1.14	1.14	1.03	1.04	1.05	1.06	1.00	1.06	1.05	1.03
T (°C)	$[Zn\text{Cl}_3(\text{H}_2\text{O})_2]^- \cdot 24\text{H}_2\text{O}$				$[Zn\text{Cl}_4]^{2-} \cdot 24\text{H}_2\text{O}$							
	A	B	C	D	A	B	C	D	A	B	C	D
0	3.56	3.45	3.09	3.23	3.10	2.99	3.00	3.07				
25	3.02	2.92	2.61	2.73	2.62	2.52	2.53	2.59				
50	2.59	2.50	2.24	2.33	2.24	2.15	2.16	2.21				
100	1.97	1.89	1.70	1.76	1.69	1.62	1.63	1.67				
200	1.24	1.19	1.07	1.11	1.06	1.02	1.02	1.05				
300	0.85	0.82	0.73	0.76	0.72	0.70	0.70	0.71				

A, B, C, and D represent different local configurations

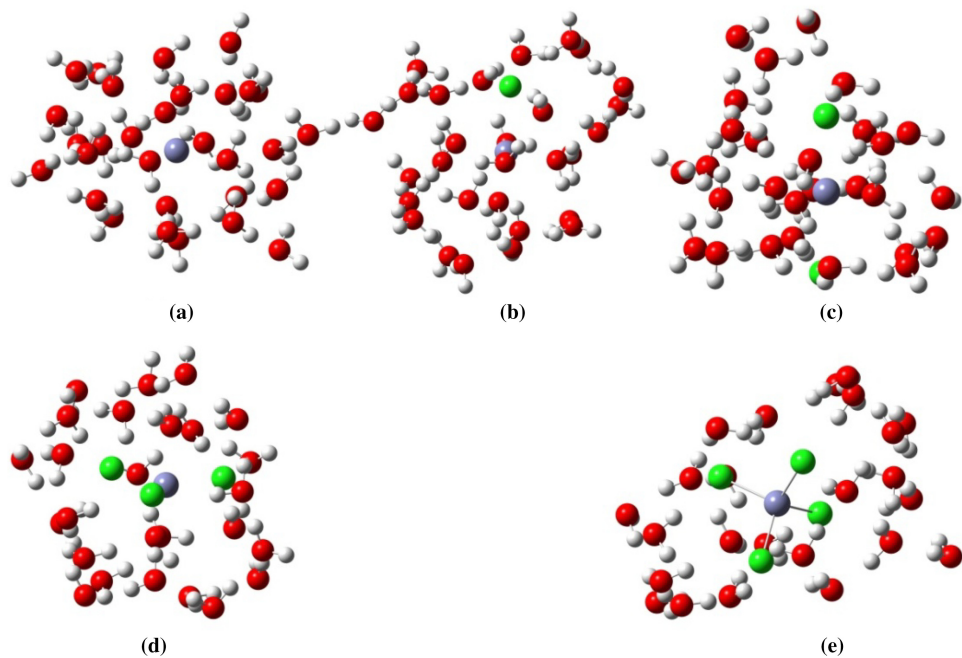


Fig. 6 Optimized structures of different species of Zn^{2+} in aqueous solutions. **a–e** represent $[\text{Zn}(\text{H}_2\text{O})_6]^{2+} \cdot 24\text{H}_2\text{O}$, $[\text{ZnCl}(\text{H}_2\text{O})_5]^+ \cdot 24\text{H}_2\text{O}$, $[\text{ZnCl}_2(\text{H}_2\text{O})_4] \cdot 24\text{H}_2\text{O}$, $[\text{ZnCl}_3(\text{H}_2\text{O})_2]^- \cdot 24\text{H}_2\text{O}$, and $[\text{ZnCl}_4]^{2-} \cdot 24\text{H}_2\text{O}$, respectively

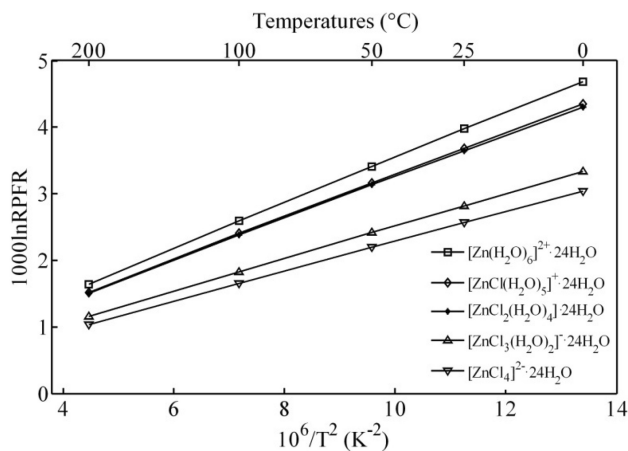


Fig. 7 Reduced partition function ratios for different species of aqueous Zn^{2+} as a function of temperature

4.74, and 4.74 (B3LYP/6-311G*) for all aqueous Zn^{2+} species studied. For all the water droplets of Zn complexes, the vibration frequencies of the structures had no negative frequencies in our method. Therefore, the results obtained in this study are reasonable compared to previous studies, which had some negative frequencies.

Table 3 Isotopic fractionation of zinc (in terms of $^{66}\text{Zn}/^{64}\text{Zn}$) between smithsonite and sphalerite

Temperature (°C)	0	25	50	100	200	300	500
$1000 * \ln \alpha$	0.64	0.55	0.48	0.37	0.24	0.17	0.09

3.3 Isotope fractionation factors of zinc between different substances

3.3.1 Zinc isotopic fractionation between different minerals

Zinc mainly exists in the minerals of sphalerite and smithsonite, which can co-exist on Earth. Therefore, investigation into the isotope fractionation factor between these two important Zn-bearing minerals could give us their formation temperature. Previous studies have reported that smithsonite may be heavier than sphalerite by up to 0.3‰ (at about 200 °C) (Albarède 2004). In this study, the calculated results suggest that smithsonite is isotopically heavier than coexisting sphalerite and the Zn isotope fractionation factor varied from 0.37 to 0.24 in the temperature range of 100–200 °C. Our results are consistent with experimental values (Table 3 and Fig. 2).

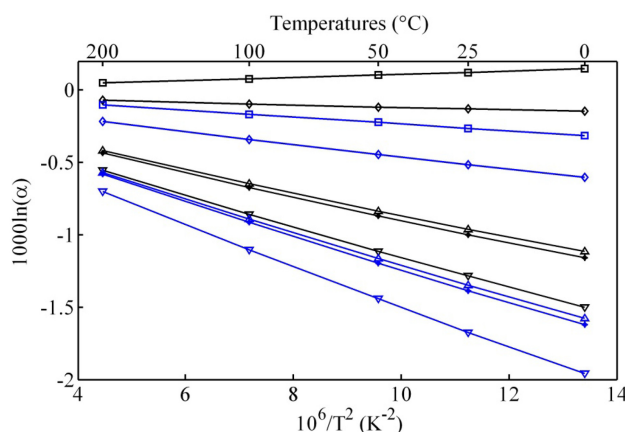


Fig. 8 Zinc isotope fractionation factors between minerals and aqueous Zn^{2+} as a function of temperature. Black lines represent sphalerite versus aqueous Zn^{2+} . Blue lines represent calcite versus aqueous Zn^{2+} . Square, diamond, upright triangle, asterisk, and inverted triangle represent $[ZnCl_4]^{2-} \cdot 24H_2O$, $[ZnCl_3(H_2O)_2]^{+} \cdot 24H_2O$, $[ZnCl_2(H_2O)_4] \cdot 24H_2O$, $[ZnCl(H_2O)_5]^{+} \cdot 24H_2O$, and $[Zn(H_2O)_6]^{2+} \cdot 24H_2O$, respectively

3.3.2 Zinc isotopic fractionation between sphalerite, calcite, and aqueous solutions

Hydrothermal ore deposits are very important due to their economic significance. Sphalerite or calcite can be precipitated from hydrothermal fluids. Kinetic (e.g., rapid precipitate) and equilibrium isotope effects occur during this process. From the investigations above, the predominant species of Zn in hydrothermal fluid are $[Zn(H_2O)_6]^{2+} \cdot 24H_2O$ and $[ZnCl_4]^{2-} \cdot 24H_2O$, and the solid phases are sphalerite and calcite. In this section, we calculated the equilibrium isotope fractionation factors between solid phases (sphalerite and calcite) and hydrothermal fluids at different temperatures (Fig. 8). The theoretical calculation results indicate that the equilibrium isotope fractionation factors between solid phases and $[Zn(H_2O)_6]^{2+} \cdot 24H_2O$ are much larger than the factors between solid phases and $[ZnCl_4]^{2-} \cdot 24H_2O$. In general, solutions enrich heavy Zn isotopes relative to solid phases except for isotope fractionation between sphalerite and $[ZnCl_4]^{2-} \cdot 24H_2O$.

4 Conclusions

This study used the first-principles DFT method (B3LYP/6-311G*) to optimize structures and calculate frequencies of a series of Zn-bearing minerals and Zn^{2+} complexes in order to determine (1) the RPFRs of their different isotopologues, and (2) the equilibrium isotope fractionation factors between these compounds. In geologic systems, Zn-bearing solutions or liquid are very important; hence, the

RPFRs of different aqueous Zn^{2+} species were calculated. In low-salinity solutions, the complexes of aqueous Zn^{2+} displayed octahedral coordination (such as $[Zn(H_2O)_6]^{2+}$), while in high salinity solutions tetrahedral coordination (such as $[ZnCl_4]^{2-}$) was observed. The results indicate that the RPFRs of different Zn^{2+} complexes decreased with chlorine increase, i.e., the RPFRs decreased in the sequence $[Zn(H_2O)_6]^{2+} \cdot 24H_2O > [ZnCl(H_2O)_5]^{+} \cdot 24H_2O > [ZnCl_2(H_2O)_4] \cdot 24H_2O > ZnCl_3(H_2O)_2^{-} \cdot 24H_2O > [ZnCl_4]^{2-} \cdot 24H_2O$.

If using gaseous $ZnCl_2$ as the Zn species during vaporization, a net Zn isotope fractionation can be deduced based on our calculation results of anorthite, forsterite, and enstatite. The calculated net Zn isotope fractionation of vaporization was about 7–7.5‰. Our theoretical calculation results show that equilibrium isotope fractionation factors could play a small role in isotope fractionation of evaporation processes. The magnitude of Zn isotope fractionation matches the experimental observations of the range of Zn isotope distribution of lunar samples (e.g., Paniello et al. 2012). Therefore, vaporization processes may be the cause of the large distribution of Zn isotope signals found on the Moon.

Furthermore, equilibrium Zn isotope fractionation between smithsonite and sphalerite were about 0.37–0.24‰ in the temperature range of 100–200 °C in good agreement with experimental data.

Acknowledgements Y.L. and co-author are grateful for support from 973 Program Fund (No. 2014CB440904), Chinese National Science Fund Projects (Nos. 41530210, 41490635, 41403051).

References

- Albarède F (2004) The stable isotope geochemistry of copper and zinc. *Rev Miner Geochem* 55:409–427
- Albarède F (2009) Volatile accretion history of the terrestrial planets and dynamic implications. *Nature* 461:1227–1233
- Anbar A, Jarzecki A, Spiro TG (2005) Theoretical investigation of iron isotope fractionation between $Fe(H_2O)_6^{2+}$ and $Fe(H_2O)_5^{2+}$: implications for iron stable isotope geochemistry. *Geochim Cosmochim Acta* 69:825–837
- Anderson AJ, Mayanovic RA, Bajt S (1995) Determination of the local structure and speciation of zinc in individual hypersaline fluid inclusions by micro-XAFS. *Can Mineral* 33:499–508
- Anderson AJ, Mayanovic RA, Bajt S (1998) A microbeam XAFS study of aqueous chlorozinc complexing to 430 degrees C in fluid inclusions from the Knaumuehl granitic pegmatite, Saxonian granulite massif, Germany. *Can Mineral* 36:511–524
- Bermin J, Vance D, Archer C, Statham P (2006) The determination of the isotopic composition of Cu and Zn in seawater. *Chem Geol* 226:280–297
- Bigeleisen J (1996) Nuclear size and shape effects in chemical reactions. Isotope chemistry of the heavy elements. *J Am Chem Soc* 118:3676–3680

- Bigeleisen J (1998) Second-order correction to the Bigeleisen–Mayer equation due to the nuclear field shift. *Proc Natl Acad Sci* 95:4808–4809
- Bigeleisen J, Mayer MG (1947) Calculation of equilibrium constants for isotopic exchange reactions. *J Chem Phys* 15:261
- Black JR, Kavner A, Schauble EA (2011) Calculation of equilibrium stable isotope partition function ratios for aqueous zinc complexes and metallic zinc. *Geochim Cosmochim Acta* 75:769–783
- Blix R, Ubisch H, Wickman FE (1957) A search for variations in the relative abundance of the zinc isotopes in nature. *Geochim Cosmochim Acta* 11:162–164
- Bol W, Gerrits G, van Panthaleon Eck C (1970) The hydration of divalent cations in aqueous solution. An X-ray investigation with isomorphous replacement. *J Appl Crystallogr* 3:486–492
- Chang TL, Zhao MT, Li WJ, Wang J, Qian QY (2001) Absolute isotopic composition and atomic weight of zinc. *Int J Mass Spectrom* 208:113–118
- Chapman S, Cowling T (1991) The mathematical theory of non-uniform gases. Cambridge University Press, Cambridge
- Chou C-L, Boynton W, Sundberg L, Wasson J (1975) Volatiles on the surface of Apollo 15 green glass and trace-element distributions among Apollo 15 soils. *Lunar Planet Sci Conf Proc* 6:1701–1727
- Cloquet C, Carignan J, Lehmann MF, Vanhaecke F (2008) Variation in the isotopic composition of zinc in the natural environment and the use of zinc isotopes in biogeosciences: a review. *Anal Bioanal Chem* 390:451–463
- Dauphas N, Rouxel O (2006) Mass spectrometry and natural variations of iron isotopes. *Mass Spectrom Rev* 25:515–550
- Davis AM, Hashimoto A, Clayton RN, Mayeda TK (1990) Isotope mass fractionation during evaporation of Mg_2SiO_4 . *Nature* 347:655–658
- Driesner T, Seward T (2000) Experimental and simulation study of salt effects and pressure/density effects on oxygen and hydrogen stable isotope liquid-vapor fractionation for 4–5 molal aqueous NaCl and KCl solutions to 400 °C. *Geochim Cosmochim Acta* 64:1773–1784
- Frisch AE, Frisch MJ, Trucks GW (2003) Gaussian 03 user's reference. Gaussian (**Incorporated**)
- Frisch M, Trucks G, Schlegel HB, Scuseria G, Robb M, Cheeseman J, Scalmani G, Barone V, Mennucci B, Petersson G (2009) Gaussian 09, Revision A. 02, vol 270. Gaussian, Inc., Wallingford, p 271
- Fujii T, Albarède F (2012) Ab initio calculation of the Zn isotope effect in phosphates, citrates, and malates and applications to plants and soil. *PLoS ONE* 7:e30726
- Fujii T, Moynier FDR, Uehara A, Abe M, Yin Q-Z, Nagai T, Yamana H (2009a) Mass-dependent and mass-independent isotope effects of zinc in a redox reaction. *J Phys Chem A* 113:12225–12232
- Fujii T, Moynier F, Albarède F (2009b) The nuclear field shift effect in chemical exchange reactions. *Chem Geol* 267:139–156
- Fujii T, Moynier F, Telouk P, Abe M (2010) Experimental and theoretical investigation of isotope fractionation of zinc between aqua, chloro, and macrocyclic complexes. *J Phys Chem A* 114:2543–2552
- Fujii T, Moynier F, Pons M-L, Albarède F (2011) The origin of Zn isotope fractionation in sulfides. *Geochim Cosmochim Acta* 75:7632–7643
- Gagnevin D, Boyce A, Barrie C, Menuge J, Blakeman R (2012) Zn, Fe and S isotope fractionation in a large hydrothermal system. *Geochim Cosmochim Acta* 88:183–198
- Gibbs GV (1982) Molecules as models for bonding in silicates. *Am Miner* 67:421–450
- He HT, Liu Y (2015) Silicon isotope fractionation during the precipitation of quartz and the adsorption of $H_4SiO_4(aq)$ on Fe(III)-oxyhydroxide surfaces. *Chin J Geochem* 34:459–468
- He HT, Zhang S, Zhu C, Liu Y (2016) Equilibrium and kinetic Si isotope fractionation factors and their implications for Si isotope distributions in the Earth's surface environments. *Acta Geochim* 35:15–24
- Hehre WJ (1986) Ab initio molecular orbital theory. *Acc Chem Res* 9:399–406
- Herzog GF, Moynier F, Albarède F, Bereznay AA (2009) Isotopic and elemental abundances of copper and zinc in lunar samples, Zagami, Pele's hairs, and a terrestrial basalt. *Geochim Cosmochim Acta* 73:5884–5904
- Herzog GF, Alexander CMOD, Berger EL, Delaney JS, Glass BP (2010) Potassium isotope abundances in Australasian tektites and microtektites. *Meteorit Planet Sci* 43:1641–1657
- Herzog GF, Albrecht A, Peixue MA, Fink D, Klein J, Middleton R, Bogard DD, Nyquist LE, Shih CY, Garrison DH (2011) Cosmic-ray exposure history of the Norton County enstatite achondrite. *Meteorit Planet Sci* 46:284–310
- Hill PS, Schauble EA, Shahar A, Tonui E, Young ED (2009) Experimental studies of equilibrium iron isotope fractionation in ferric aquo-chloro complexes. *Geochim Cosmochim Acta* 73:2366–2381
- Humayun M, Clayton RN (1995) Potassium isotope cosmochemistry: genetic implications of volatile element depletion. *Geochim Cosmochim Acta* 59:2131–2148
- Jarzecki A, Anbar A, Spiro T (2004) DFT analysis of $Fe(H_2O)_6^{3+}$ and $Fe(H_2O)_6^{2+}$ structure and vibrations; implications for isotope fractionation. *J Phys Chem A* 108:2726–2732
- John SG, Rouxel OJ, Craddock PR, Engwall AM, Boyle EA (2008) Zinc stable isotopes in seafloor hydrothermal vent fluids and chimneys. *Earth Planet Sci Lett* 269:17–28
- Kruh R, Standley C (1962) An X-ray diffraction study of aqueous zinc chloride solutions. *Inorg Chem* 1:941–943
- Li XF, Liu Y (2010) First-principles study of Ge isotope fractionation during adsorption onto Fe(III)-oxyhydroxide surfaces. *Chem Geol* 278:15–22
- Li X, Liu Y (2011) Equilibrium Se isotope fractionation parameters: a first-principles study. *Earth Planet Sci Lett* 304:113–120
- Li X, Liu Y (2015) A theoretical model of isotopic fractionation by thermal diffusion and its implementation on silicate melts. *Geochim Cosmochim Acta* 154:18–27
- Li X, Zhao H, Tang M, Liu Y (2009) Theoretical prediction for several important equilibrium Ge isotope fractionation factors and geological implications. *Earth Planet Sci Lett* 287:1–11
- Liu Y, Tossell JA (2005) Ab initio molecular orbital calculations for boron isotope fractionations on boric acids and borates. *Geochim Cosmochim Acta* 69:3995–4006
- Liu Y, Olsen AA, Rimstidt JD (2006) Mechanism for the dissolution of olivine series minerals in acidic solutions. *Am Miner* 91:455–458
- Liu Q, Tossell JA, Liu Y (2010) On the proper use of the Bigeleisen–Mayer equation and corrections to it in the calculation of isotopic fractionation equilibrium constants. *Geochim Cosmochim Acta* 74:6965–6983
- Liu X, Lu X, Wang R, Meijer EJ (2011) Understanding hydration of Zn^{2+} in hydrothermal fluids with ab initio molecular dynamics. *Phys Chem Chem Phys* 13:13305–13309
- Lodders K (2003) Solar system abundances and condensation temperatures of the elements. *Astrophys J* 591:1220–1247
- Luck JM, Othman DB, Albarède F (2005) Zn and Cu isotopic variations in chondrites and iron meteorites: early solar nebula reservoirs and parent-body processes. *Geochim Cosmochim Acta* 69:5351–5363
- Luck J, Ben Othman D, Zanda B, Albarède F (2006) Zn Cu isotopes in chondritic components. *Geochim Cosmochim Acta Suppl* 70:373

- Magini M, Licheri G, Paschina G, Piccaluga G, Pinna G (1988) X-ray diffraction of ions in aqueous solutions: hydration and complex formation. CRC Press, Boca Raton
- Maréchal C, Albarède F (2002) Ion-exchange fractionation of copper and zinc isotopes. *Geochim Cosmochim Acta* 66:1499–1509
- Maréchal CN, Télouk P, Albarède F (1999) Precise analysis of copper and zinc isotopic compositions by plasma-source mass spectrometry. *Chem Geol* 156:251–273
- Mason TFD, Weiss DJ, Chapman JB, Wilkinson JJ, Tessalina SG, Spiro B, Horstwood MSA, Spratt J, Coles BJ (2005) Zn and Cu isotopic variability in the Alexandrinka volcanic-hosted massive sulphide (VHMS) ore deposit, Urals, Russia. *Chem Geol* 221:170–187
- Mayanovic R, Anderson A, Bassett W, Chou I (1999) XAFS measurements on zinc chloride aqueous solutions from ambient to supercritical conditions using the diamond anvil cell. *J Synchrotron Radiat* 6:195–197
- Moynier F, Albarède F, Herzog GF (2006) Isotopic composition of zinc, copper, and iron in lunar samples. *Geochim Cosmochim Acta* 70:6103–6117
- Moynier F, Blachert-Toft J, Telouk P, Luck J-M, Albarède F (2007) Comparative stable isotope geochemistry of Ni, Cu, Zn, and Fe in chondrites and iron meteorites. *Geochim Cosmochim Acta* 71:4365–4379
- Moynier F, Pichat S, Pons M-L, Fike D, Balter V, Albarède F (2009) Isotopic fractionation and transport mechanisms of Zn in plants. *Chem Geol* 267:125–130
- Moynier F, Beck P, Yin Q-Z, Ferroir T, Barrat J-A, Paniello R, Telouk P, Gillet P (2010) Volatilization induced by impacts recorded in Zn isotope composition of ureilites. *Chem Geol* 276:374–379
- Moynier F, Paniello RC, Gounelle M, Albarède F, Beck P, Podosek F, Zanda B (2011) Nature of volatile depletion and genetic relationships in enstatite chondrites and aubrites inferred from Zn isotopes. *Geochim Cosmochim Acta* 75:297–307
- Novak M, Sipkova A, Chrastny V, Stepanova M, Voldrichova P, Veselovsky F, Prechova E, Blaha V, Curik J, Farkas J (2016) Cu-Zn isotope constraints on the provenance of air pollution in Central Europe: using soluble and insoluble particles in snow and rime. *Environ Pollut* 218:1135–1146
- Oi T (2000) Ab initio molecular orbital calculations of reduced partition function ratios of polyboric acids and polyborate anions. *Z Naturforsch A* 55:623–628
- Oi T, Yanase S (2001) Calculations of reduced partition function ratios of hydrated monoborate anion by the ab initio molecular orbital theory. *J Nucl Sci Technol* 38:429–432
- Otake T, Lasaga AC, Ohmoto H (2008) Ab initio calculations for equilibrium fractionations in multiple sulfur isotope systems. *Chem Geol* 249:357–376
- Palme H, Larimer J, Lipschutz M (1988) Moderately volatile elements. *Meteor Early Sol Syst* 1:436–461
- Paniello RC, Day JMD, Moynier F (2012) Zinc isotopic evidence for the origin of the Moon. *Nature* 490:376–379
- Parchment OG, Vincent MA, Hillier IH (1996) Speciation in aqueous zinc chloride. An ab initio hybrid microsolvation/continuum approach. *J Phys Chem* 100:9689–9693
- Paschina G, Piccaluga G, Pinna G, Magini M (1983) Chloro-complexes formation in a ZnCl–CdCl aqueous solution: an X-ray diffraction study. *J Chem Phys* 78:5745
- Pons ML, Fujii T, Rosing M, Quitté G, Télouk P, Albarède F (2013) A Zn isotope perspective on the rise of continents. *Geobiology* 11:201–214
- Ponzevera E, Quétel CR, Berglund M, Taylor PDP, Evans P, Loss RD, Fortunato G (2006) Mass discrimination during MC-ICPMS isotopic ratio measurements: investigation by means of synthetic isotopic mixtures (IRMM-007 series) and application to the calibration of natural-like zinc materials (including IRMM-3702 and IRMM-651). *J Am Soc Mass Spectrom* 17:1412–1427
- Richet P, Bottinga Y, Janoy M (1977) A review of hydrogen, carbon, nitrogen, oxygen, sulphur, and chlorine stable isotope enrichment among gaseous molecules. *Annu Rev Earth Planet Sci* 5:65–110
- Richter FM, Davis AM, Ebel DS, Hashimoto A (2002) Elemental and isotopic fractionation of type B calcium-, aluminum-rich inclusions: experiments, theoretical considerations, and constraints on their thermal evolution. *Geochim Cosmochim Acta* 66:521–540
- Richter FM, Janney PE, Mendybaev RA, Davis AM, Wadhwa M (2007) Elemental and isotopic fractionation of Type B CAI-like liquids by evaporation. *Geochim Cosmochim Acta* 71:5544–5564
- Richter FM, Dauphas N, Teng F-Z (2009) Non-traditional fractionation of non-traditional isotopes: evaporation, chemical diffusion and Soret diffusion. *Chem Geol* 258:92–103
- Rosman KJR (1972) A survey of the isotopic and elemental abundance of zinc. *Geochim Cosmochim Acta* 36:801–819
- Rustad JR, Bylaska EJ (2007) Ab initio calculation of isotopic fractionation in $B(OH)_3(aq)$ and $BOH_4^-(aq)$. *J Am Chem Soc* 129:2222–2223
- Rustad JR, Zarzycki P (2008) Calculation of site-specific carbon-isotope fractionation in pedogenic oxide minerals. *Proc Natl Acad Sci* 105:10297–10301
- Rustad JR, Nelmes SL, Jackson VE, Dixon DA (2008) Quantum-chemical calculations of carbon-isotope fractionation in $CO_2(g)$, aqueous carbonate species, and carbonate minerals. *J Phys Chem A* 112:542–555
- Rustad JR, Casey WH, Yin QZ, Bylaska EJ, Felmy AR, Bogatko SA, Jackson VE, Dixon DA (2010) Isotopic fractionation of $Mg^{2+}(aq)$, $Ca^{2+}(aq)$, and $Fe^{2+}(aq)$ with carbonate minerals. *Geochim Cosmochim Acta* 74:6301–6323
- Schauble E (2003) Modeling zinc isotope fractionations. *Agu Fall Meet* 1:0781
- Schauble EA (2004) Applying stable isotope fractionation theory to new systems. *Rev Mineral Geochem* 55:65–111
- Schauble EA (2007) Role of nuclear volume in driving equilibrium stable isotope fractionation of mercury, thallium, and other very heavy elements. *Geochim Cosmochim Acta* 71:2170–2189
- Schauble EA, Ghosh P, Eiler JM (2006) Preferential formation of $^{13}C-^{18}O$ bonds in carbonate minerals, estimated using first-principles lattice dynamics. *Geochim Cosmochim Acta* 70:2510–2529
- Seo JH, Lee SK, Lee I (2007) Quantum chemical calculations of equilibrium copper (I) isotope fractionations in ore-forming fluids. *Chem Geol* 243:225–237
- Tanimizu M, Asada Y, Hirata T (2002) Absolute isotopic composition and atomic weight of commercial zinc using inductively coupled plasma mass spectrometry. *Anal Chem* 74:5814
- Taylor SR, McLennan SM (1995) The geochemical evolution of the continental crust. *Rev Geophys* 33:241–265
- Tossell J (2005) Calculating the partitioning of the isotopes of Mo between oxidic and sulfidic species in aqueous solution. *Geochim Cosmochim Acta* 69:2981–2993
- Urey HC (1947) The thermodynamic properties of isotopic substances. *J Chem Soc* 562:562–581
- Vance D, Archer C, Bermin J, Kennaway G, Cox EJ, Statham PJ, Lohan MC, Ellwood MJ (2006) Zn isotopes as a new tracer of metal micronutrient usage in the oceans. *Geochim Cosmochim Acta* 70:A666
- Wai CM, Wasson JT (1977) Nebular condensation of moderately volatile elements and their abundances in ordinary chondrites. *Earth Planet Sci Lett* 36:1–13
- Weiss DJ, Rausch N, Mason TFD, Coles BJ, Wilkinson JJ, Ukonmaanaho L, Arnold T, Nieminen TM (2007) Atmospheric

- deposition and isotope biogeochemistry of zinc in ombrotrophic peat. *Geochim Cosmochim Acta* 71:3498–3517
- Wilkinson J, Weiss D, Mason T, Coles B (2005) Zinc isotope variation in hydrothermal systems: preliminary evidence from the Irish Midlands ore field. *Econ Geol* 100:583–590
- Young ED, Galy A (2004) The isotope geochemistry and cosmochemistry of magnesium. *Rev Mineral Geochem* 55:197–230
- Zeebe RE (2005) Stable boron isotope fractionation between dissolved $\text{B}(\text{OH})_3$ and $\text{B}(\text{OH})_4^-$. *Geochim Cosmochim Acta* 69:2753–2766
- Zhu X, Guo Y, Williams R, O’nions R, Matthews A, Belshaw N, Canters G, De Waal E, Burgess U, Burgess B (2002) Mass fractionation processes of transition metal isotopes. *Earth Planet Sci Lett* 200:47–62